Electric Power Systems Research 190 (2021) 106773

Contents lists available at ScienceDirect

Electric Power Systems Research

journal homepage: www.elsevier.com/locate/epsr

Reduced-order modeling of inverter-based generation using hybrid singular perturbation

Ivo Caduff[*,a], Uros Markovic[a], Ciaran Roberts[b], Gabriela Hug[a], Evangelos Vrettos[b]

[a] EEH - Power Systems Laboratory, ETH Zurich, Physikstrasse 3, Zurich 8092, Switzerland
[b] Lawrence Berkeley National Laboratory, 1 Cyclotron Rd, Berkeley, CA 94720, USA

ARTICLE INFO

Keywords:
Inverter dynamics
Singular perturbation
Hybrid method
Participation factors
Model-order reduction

ABSTRACT

This paper contributes to the field of inverter modelling for large-scale simulations by introducing a novel Model-Order Reduction (MOR) method based on singular perturbation. Motivated by the timescale separation between the fast and slow dynamics in an inverter-based power system, the proposed nonlinear MOR concept extends on the existing zero- and first-order reduction methods by combining the low computational burden of the former approach with the higher accuracy of the latter one. As a result, such hybrid MOR technique preserves the slow system dynamics of the full-order model, while simultaneously capturing the impact of the removed fast states on slow variables. Moreover, we introduce several improvements to the existing first-order MOR in order to make it tractable and more efficient when applied to a realistic full-order inverter model. The novel hybrid approach is applied to both grid-forming and grid-following inverter control schemes, and compared against existing reduction methods from the literature. The results showcase a better time-domain performance of the hybrid method during transients, while having a negligible increase in computational requirements compared to the traditional zero-order approach.

1. Introduction and motivation

With increasing shares of inverter-interfaced renewable energy resources such as photovoltaics and variable-speed wind turbines, dynamic power system simulations are facing new challenges [1]. One of these challenges consists of finding the appropriate amount of detail for individual inverter models depending on the application. For microgrid applications there exists a commonly used inverter model that captures both the outer and inner cascaded control loops and has been used in various studies in the literature [2–7]. Applications include stability analyses [2–4], comparison of different active power control algorithms [4–6], as well as the evaluation of dynamic interactions between inverters and synchronous machines [7]. Nonetheless, the existing model is too complex for use in large-scale simulations due to the large number of dynamic variables, which motivates employing Model Order Reduction (MOR) methods to enhance scalability.

A commonly used MOR approach in power system modeling is singular perturbation, which is based on timescale separation of fast and slow dynamics and assumes that the fast states reach a quasi steady-state instantaneously [8]. Several MOR methods based on singular perturbation have recently been proposed to simplify inverter models [9–14]. The authors in Kodra et al. [9] employ direct truncation and compare it against reduction models based on particle swarm optimization. However, they focus on reducing a simplified sixth-order inverter model that initially does not encapsulate all of the underlying control dynamics. Similarly, the inverter models used in Mariani et al. [10] and [11] for stability assessment of a reduced-order islanded microgrid are too simplistic, with the former study ignoring the effect of filter dynamics and the latter neglecting the fast inner loop controllers essential for stable converter operation. This is improved in Rasheduzzaman et al. [12], where a detailed 15th-order model is considered, both in the islanded and grid-connected mode, and subsequently reduced to an eighth-order model by neglecting the fast dynamics of states associated with the voltage and current measurements in the *RLC* filter and the filter state of the Phase-Locked Loop (PLL). Interestingly, the dynamics of the traditionally “fast” inner control loops are preserved in the reduced model due to unconventional parametrization of the associated PI controllers which might not be justified in real-world applications. While the computational benefits and steady-state tracking of the proposed low-order model are validated, the fast transients are not captured. Moreover, all aforementioned studies deal with linearized inverter models limited to an operating region close to the equilibrium, which implies that the obtained reduced-order models might not have a satisfactory performance during

* Corresponding author.
E-mail address: icaduff@gmail.com (I. Caduff).

https://doi.org/10.1016/j.epsr.2020.106773
Received 4 October 2019; Received in revised form 20 April 2020; Accepted 2 August 2020
Available online 30 August 2020

large disturbances.

In contrast, [13] and [14] focus on large-scale, nonlinear dynamic models of low-inertia systems. The work in Luo and Dhople [13] applies singular perturbation and Kron reduction to the model of a 100% inverter-based islanded microgrid with the aim of reducing its model order in temporal and spatial aspects, respectively. Individual inverters are reduced to a fifth-order model by eliminating the dynamical equations for the voltage and current controllers through means of singular perturbation. MOR is taken a step further in this study by also proposing third- and first-order models in the context of different applications such as design and verification of secondary and tertiary-level controllers, long-term performance and reliability evaluation, respectively. However, the inverter model used in Luo and Dhople [13] excludes the filter capacitors and the case studies are solely confined to small-signal disturbances in the form of load resistance step changes (corresponding to active power mismatch), and are therefore not reflective of transient capabilities of the given inverter models. On the other hand, [14] proposes a reduced-order model of a low-inertia system comprising power converters, synchronous generators and their interactions with the power grid (i.e., network dynamics). Using arguments from singular perturbation theory, the authors obtain a tractable model for control design and subsequently use the insights gained to bridge the gap between grid-level objectives and device-level control by introducing an internal model and matching controller that exploits structural similarities between power converters and synchronous generators. In addition, they propose a nonlinear droop control that stabilizes the power system. Nevertheless, the converter control scheme does not include inner controllers and PLL dynamics, and it does not study the accuracy of the reduced model during large disturbances.

Guided by a standard practice in singular perturbation, all previous MOR strategies exploit *small parameters* to identify the fast and slow states. More precisely, the states "to be removed" are determined based on the time constants of their respective differential equations. Such approach is meaningful when capturing slow system dynamics, as it preserves stability properties of the original system within the reduced-order model [15,16]. However, it discards the dynamics of the fast states and therefore some potentially important phenomena during transients, as indicated by the results in Rasheduzzaman et al. [12], Cossart et al. [17]. Nevertheless, depending on the model application, some relevant fast dynamics might be of interest (e.g., internal PLL dynamics during active power transients) and should not be completely neglected. This idea is partially addressed in Cossart et al. [17] where, instead of employing small parameters, singular perturbation is performed based on modal analysis and participation factors. Such approach investigates a timescale separation between different modes in the system and identifies the states to be removed by their contribution to the fast modes. The authors obtain several reduced-order inverter control designs in nonlinear form and demonstrate that even the models of very low order suffice when analyzing steady-state performance. However, the time-domain responses reveal a significant loss in model accuracy when subjected to a large disturbance, independent of the model order.

Alternatively, the work in Vorobev et al. [18] takes into account transmission line dynamics when performing singular perturbation of an inverter-based microgrid, justified by the fact that the line and simplified inverter dynamics are on similar timescales. The study even suggests that the timescale separation is not large enough to apply the standard singular perturbation method. Therefore, a new approach called *first-order singular perturbation* is introduced and demonstrated on a small test system. As opposed to neglecting the dynamics of fast variables altogether, this method allows for a more accurate inclusion of possible effects that the fast states could have on slow modes. Nevertheless, the proposed approach relies on small parameters and uses an oversimplified, linear, fifth-order inverter model as an initial full-order benchmark. As a result, the authors propose a reduced third-order model that could be of interest for the purposes of small-signal analysis, but cannot track transients under large disturbances.

This paper continues the previous line of research and extends it by proposing a novel *hybrid* method for singular perturbation-based MOR. Specifically, the presented method combines the classical approach used in Kodra et al. [9], Mariani et al. [10], Iyer et al. [11], Rasheduzzaman et al. [12], Luo and Dhople [13], Curi et al. [14], Cossart et al. [17] (called *Zero-Order Singular Perturbation (ZOSP)* hereinafter) with the first-order approach of [18] in order to achieve a trade-off between the transient performance and model complexity. Furthermore, we introduce two additional improvements to [18]. First, we apply the *First-Order Singular Perturbation (FOSP)* method directly to the detailed nonlinear model instead of a simplified linear model, resulting in more accurate lower-order inverter representation; and second, we use modal analysis (i.e., participation factors) instead of small parameters to determine the order of the dynamic variables to be removed. However, unlike the approach in Cossart et al. [17], where the linearization and modal analysis have been conducted only once on the level of the full-order model, we repeat modal analysis in an iterative fashion after the removal of each dynamic state. The proposed hybrid method enables separation of the nonlinear model at hand into three timescales, thereby increasing flexibility in the reduction process and achieving a better trade-off between complexity and performance. Unlike the previous studies, we evaluate the effectiveness of our model-reduction approach on both the grid-forming and grid-following converter control schemes, due to the differences in system dynamics in the presence of a PLL.

The rest of the paper is structured as follows. In Section 2, the theoretical preliminaries of singular perturbation are introduced, together with the analytical formulation of both the zero- and first-order approach in linear and nonlinear form respectively. Furthermore, the mathematical concepts of the proposed hybrid singular perturbation method are described, including the iterative participation factor analysis. The state-of-the-art converter control scheme and the timescale separation pertaining to such control and low-pass filter design are presented and discussed in Section 3. Subsequently, Section 4 showcases different model orders obtained via the hybrid approach and compares them against the traditional zero-order-reduced models in terms of time-domain and small-signal stability performance. Finally, Section 5 draws the main conclusions and discusses the outlook of the study.

2. Methodology and analytical formulation

2.1. Singular perturbation principles

For better understanding of the employed MOR method, we first introduce basic theoretical preliminaries of singular perturbation adopted from [16]. Let us consider a singular perturbation model of a nonlinear, time-invariant system

$$\dot{x}_s = f(x_s, x_f, u), \quad x_s(t_0) = x_s^0, \tag{1a}$$

$$\epsilon\dot{x}_f = g(x_s, x_f, u), \quad x_f(t_0) = x_f^0, \tag{1b}$$

where $x_s \in \mathbb{R}^n$, $x_f \in \mathbb{R}^m$ and $u \in \mathbb{R}^r$ are the state vectors describing the "slow" and "fast" states and the control input vector, respectively, and $f(\cdot)$ and $g(\cdot)$ are assumed to be sufficiently many times continuously differentiable functions of their arguments. The small positive scalar $\epsilon \in \mathbb{R}_{>0}$ in (1b) multiplies the derivatives of the fast states - representing the small parameters - to be neglected. Let $(x_s^0, x_f^0) \in \mathbb{R}^{n+m}$ be the equilibrium state of the nonlinear singularly perturbed system (1) and $u^0 \in \mathbb{R}^r$ be a constant control input such that

$$f(x_s^0, x_f^0, u^0) = \mathbf{0}_n, \tag{2a}$$

$$g(x_s^0, x_f^0, u^0) = \mathbf{0}_m, \tag{2b}$$

and linearize the system around (x_s^0, x_f^0, u^0), as follows:

$$\Delta\dot{x}_s = A_{ss}\Delta x_s + A_{sf}\Delta x_f + B_s\Delta u, \tag{3a}$$

$$\epsilon\Delta\dot{x}_f = A_{fs}\Delta x_s + A_{ff}\Delta x_f + B_f\Delta u. \tag{3b}$$

Here, $A_{ss} \in \mathbb{R}^{n\times n}$, $A_{sf} \in \mathbb{R}^{n\times m}$, $A_{fs} \in \mathbb{R}^{m\times n}$, $A_{ff} \in \mathbb{R}^{m\times m}$, $B_s \in \mathbb{R}^{n\times r}$, $B_f \in \mathbb{R}^{m\times r}$ is the respective state-space representation, and Δ denotes a small deviation

$$\Delta x_s = x_s - x_s^0, \quad \Delta x_f = x_f - x_f^0, \quad \Delta u = u - u^0 \tag{4}$$

about the equilibrium (x_s^0, x_f^0, u^0). Note that for column vectors $x \in \mathbb{R}^n$ and $y \in \mathbb{R}^m$ we use $(x, y) = [x^\top, y^\top]^\top \in \mathbb{R}^{n+m}$ to denote a stacked vector.

The analysis of two-timescale properties of model (3) can be done by disregarding the control input ($\Delta u = \mathbb{0}_r$) and introducing a set of coordinates in which the system appears in a distinct block-triangular form. In this so-called actuator form, the fast block defined by the state vector

$$\eta = \Delta x_f + L(\epsilon)\Delta x_s \tag{5}$$

"drives" the slow block with the original state vector x_s [16, Section 1.4]. This change of variables transforms (3) into an upper-triangular form

$$\begin{bmatrix} \Delta\dot{x}_s \\ \epsilon\dot{\eta} \end{bmatrix} = \begin{bmatrix} A_{ss} - A_{sf}L & A_{sf} \\ \mathbb{0} & A_{ff} + \epsilon L A_{sf} \end{bmatrix} \begin{bmatrix} \Delta x_s \\ \eta \end{bmatrix}, \tag{6}$$

provided that the matrix $L(\epsilon) \in \mathbb{R}^{m\times n}$ satisfies the algebraic equation (see [16, Section 2 (Lemma 2.1)])

$$A_{fs} - A_{ff}L(\epsilon) + \epsilon L(\epsilon)A_{ss} - \epsilon L(\epsilon)A_{sf}L(\epsilon) = \mathbb{0}. \tag{7}$$

Separating the system (3) into two lower-order subsystems of different timescales allows us to infer the stability of the original system by analyzing the lower-order systems separately, which is of great practical significance for control analysis and design. In particular, assuming that A_{ff} exists and A_{ff} and $(A_{ss} - A_{sf}A_{ff}^{-1}A_{fs})$ are Hurwitz matrices, we can approximate the $\epsilon\Delta\dot{x}_f$ term in (3b) using a Taylor representation and reduce the order of the system. The remainder of this section discusses several such approximations.

2.2. Zero-order singular perturbation

The idea of ZOSP is to completely disregard the fast state dynamics, justified by the fact that they are occurring on a much shorter timescale compared to the slow dynamics. In other words, the changes in the fast variables can be seen as instantaneous from the perspective of slow variables. The two-timescale linear system (3) can thus be rewritten as

$$\Delta\dot{x}_s = A_{ss}\Delta x_s + A_{sf}\Delta x_f + B_s\Delta u, \tag{8a}$$

$$0_m \approx \mathrm{Y}\Delta\dot{x}_f = A_{fs}\Delta x_s + A_{ff}\Delta x_f + B_f\Delta u, \tag{8b}$$

with $\mathrm{Y} = \mathrm{diag}(\epsilon_1, \ldots, \epsilon_m)$ denoting a diagonal matrix comprised of small parameters. Note that unlike the formulation in (3b), where first derivatives of the fast states were multiplied by a common scalar ϵ, in (8b) each state variable has its own scaling factor reflecting the characteristic time constant of the respective differential equation.

The zero-order model reduction is performed by transforming differential Eq. (8b) into algebraic ones. In order to bring the system to its final (i.e., reduced) Ordinary Differential Equation (ODE) form, the algebraic expressions are solved for their respective variables

$$\Delta x_f = -A_{ff}^{-1}A_{fs}\Delta x_s - A_{ff}^{-1}B_f\Delta u, \tag{9}$$

and subsequently substituted into (8a), which yields

$$\Delta\dot{x}_s = (A_{ss} - A_{sf}A_{ff}^{-1}A_{fs})\Delta x_s + (B_s - A_{sf}A_{ff}^{-1}B_f)\Delta u. \tag{10}$$

In comparison to the initial system (8), the formulation in (10) reveals that the formerly fast states are no longer present in the reduced-order model. Nevertheless, the relations between fast and slow states act as algebraic constraints for the remaining differential states and are represented by submatrices A_{sf}, A_{ff} and A_{fs} of the initial state space. The state matrix of the reduced-order model is therefore defined as $(A_{ss} - A_{sf}A_{ff}^{-1}A_{fs})$, under the assumption that A_{ff} is nonsingular.

The same ZOSP approach can also be applied directly to nonlinear systems. Similar to the linear case, the two-timescale, nonlinear ODE system (1) can be approximated by

$$\dot{x}_s = f(x_s, x_f, u), \tag{11a}$$

$$\mathbb{0}_m \approx \mathrm{Y}\dot{x}_f = g(x_s, x_f, u), \tag{11b}$$

by assuming a quasi steady-state of the fast states. Therefore, original ODEs are converted into a set of Differential Algebraic Equations (DAEs), with algebraic equations given by the right-hand side of (11b). Depending on the complexity of the newly formed algebraic equations, it might or might not be possible to solve (11b) for the fast states and substitute the acquired expressions into (11a) in order to obtain a reduced-order ODE set. Note that a pure ODE system would be favorable for most numerical solvers, since the presence of algebraic constraints introduces additional iterations and may significantly increase computational time.

2.3. First-order singular perturbation

We demonstrate the principles of FOSP on a linear system (3) by following the derivation provided in Vorobev et al. [18]. Unlike in the traditional zero-order approach, where fast dynamics are completely neglected by converting the corresponding differential equations into algebraic ones, the first-order method removes the fast states by stating that the first derivative of Δx_f is non-zero, whereas its second derivative is negligible. This property is especially useful in systems with several distinctive timescales and has a potential of better capturing the impact of fast states on slow system dynamics. Mathematically speaking, this corresponds to a Taylor series expansion of the vector of the fast states and hence the name first-order reduction.

Let us start from a general two-timescale representation

$$\Delta\dot{x}_s = A_{ss}\Delta x_s + A_{sf}\Delta x_f + B_s\Delta u, \tag{12a}$$

$$\mathrm{Y}\Delta\dot{x}_f = A_{fs}\Delta x_s + A_{ff}\Delta x_f + B_f\Delta u, \tag{12b}$$

where, in contrast to (8), $\mathrm{Y}\Delta\dot{x}_f \neq \mathbb{0}_m$. Taking the derivative of (12b) with respect to time and equating it to zero yields

$$\mathbb{0}_m \approx \mathrm{Y}\Delta\ddot{x}_f = A_{fs}\Delta\dot{x}_s + A_{ff}\Delta\dot{x}_f + B_f\Delta\dot{u}. \tag{13}$$

Assuming time-invariant control inputs ($\Delta\dot{u} = \mathbb{0}_r$) and solving (13) for $\Delta\dot{x}_f$ results in

$$\Delta\dot{x}_f = -A_{ff}^{-1}A_{fs}\Delta\dot{x}_s. \tag{14}$$

Substituting the intermediate result (14) into (12b) gives the following expression for Δx_f:

$$\Delta x_f = -A_{ff}^{-1}\mathrm{Y}A_{ff}^{-1}A_{fs}\Delta\dot{x}_s - A_{ff}^{-1}A_{fs}\Delta x_s - A_{ff}^{-1}B_f\Delta u. \tag{15}$$

Finally, by substituting (15) into (12a) and separating the terms for Δx and $\Delta\dot{x}$, a linear first-order ODE form is obtained:

$$\dot{x}_s = A_0\Delta x_s + B_0\Delta u, \tag{16a}$$

with the reduced-order state space (A_0, B_0) defined by

$$A_0 := (I + A_{sf}A_{ff}^{-1}\mathrm{Y}A_{ff}^{-1}A_{fs})^{-1}(A_{ss} - A_{sf}A_{ff}^{-1}A_{fs}), \tag{16b}$$

$$B_0 := (I + A_{sf}A_{ff}^{-1}\mathrm{Y}A_{ff}^{-1}A_{fs})^{-1}(B_s - A_{sf}A_{ff}^{-1}B_f). \tag{16c}$$

A comparison between (16) and the corresponding ZOSP formulation in (10) reveals an addition of a new term $(I + A_{sf}A_{ff}^{-1}\mathrm{Y}A_{ff}^{-1}A_{fs})^{-1}$ to matrices A_0 and B_0. On one hand, it results in a more accurate reduced-order model, but on the other hand leads to a model representation of higher complexity which might increase computational time. Note that the reduced model is only attainable and valid if the aforementioned

inverse matrix exists.

2.4. Hybrid singular perturbation

The main idea of the proposed hybrid method is to combine ZOSP and FOSP in systems with more than two distinctive timescales and potentially better capture the dynamical performance during transients. Specifically, we consider a three-timescale, nonlinear ODE system of the form

$$\dot{x}_s = f(x, u), \quad \dot{x}_f = g(x, u), \quad \dot{x}_v = h(x, u), \tag{17}$$

where x: $=(x_s, x_f, x_v) \in \mathbb{R}^{n+m+p}$ represents the state vector comprised of slow states $x_s \in \mathbb{R}^n$, fast states $x_f \in \mathbb{R}^m$ and very fast states $x_v \in \mathbb{R}^p$, and $f(\cdot)$, $g(\cdot)$ and $h(\cdot)$ are the respective functions. Based on the discussion in Section 2.1, the dynamics of the slow states remain intact, the dynamics of the fast states are reduced using FOSP ($\dot{x}_f = \mathbf{0}$), and the dynamics of the very fast states are reduced using ZOSP ($\dot{x}_v = \mathbf{0}$), which yields the following DAE system:

$$\dot{x}_s = f(x, y, u), \tag{18a}$$

$$\mathbf{0}_m = \frac{\partial g(x, y, u)}{\partial x_s} f(x, y, u) + \frac{\partial g(x, y, u)}{\partial x_f} g(x, y, u) + \frac{\partial g(x, y, u)}{\partial x_v} h(x, y, u), \tag{18b}$$

$$\mathbf{0}_p = h(x, y, u). \tag{18c}$$

It can be seen that the hybrid method introduces two separate sets of algebraic constraints, namely (18b) and (18c), correlating the algebraic variables $y := (x_f, x_v)$ that comprise the original fast and very fast states to the preserved slow differential states $x := x_s$ in (18a). Hence, the final model order is n, i.e., it is reduced by $m + p$ compared to the original system. Note that the values of n and m do not necessarily correspond to the values of the same parameters in Section 2.1.

By applying the hybrid approach one clearly assumes a three-timescale separation, i.e., the fact the state dynamics can be split into slow, fast and very fast. For systems comprising two distinctive timescales, such classification is traditionally done based on the small parameters. However, a tri-level categorization is more complex and it might not be clear how to conduct it *a priori*. Moreover, the goal of this study is not only to preserve the slow variables but also to determine the most relevant dynamics to be preserved in order to capture the transient oscillations and overshoot. Therefore, the employed method is not based on small parameters but rather on performing an iterative Participation Factor Analysis (PFA).

2.5. Iterative participation factor analysis

PFA is an established method for quantifying the influence of a state on a mode and vice versa [19]. The knowledge of timescales gained through eigenvalue analysis, in combination with the acquired information about the coupling of states and modes, allows for classification (i.e., separation) of state variables based on the respective timescales. For a linear, time invariant ODE system

$$\dot{x} = Ax + Bu, \tag{19}$$

the participation of state k (x_k) in mode i (λ_i) is defined as

$$P_{ki} = u_{ki} v_{ki}, \tag{20}$$

where u_{ki} is the ith entry of the kth left eigenvector and v_{ki} is the ith entry of the kth right eigenvector of the state-space matrix A.

As stated in Section 1, the PFA has been used in the literature to distinguish the fast from the slow states [17]. Note that the full-order model is linearized only once at the beginning of the MOR process in Cossart et al. [17]. As a result, the participation factors are computed only once and based on their values the order of the states to be removed is determined in a single step. In contrast, this work proposes an alternative, iterative approach to PFA that involves sequential computation of participation factors as the order of the model is being reduced. More precisely, after removing each state, the newly obtained nonlinear model is linearized, PFA is performed, and the next fastest state to be removed is determined. This procedure is repeated until the desired model order is reached.

The benefit of iterative PFA is better tracking of changes in the model structure due to reduction, which can influence the systems modes in subsequent reduction steps. In other words, re-linearization of the nonlinear model at each reduction step allows to obtain a more accurate linear model approximation. It should be noted though that, as the model order progressively decreases, it becomes more likely that the state matrix of a reduced model becomes singular (due to one or more eigenvalues being zero), which of course means that the iterative process has to be stopped and the lowest possible model order has been reached.

3. System modeling and control implementation

3.1. Converter control scheme

The complete modeling and analysis of converter control is implemented in a Synchronously-rotating Reference Frame (SRF) and in per unit. The proposed control model depicted in Fig. 1 is based on a state-of-the-art Voltage Source Converter (VSC) control scheme

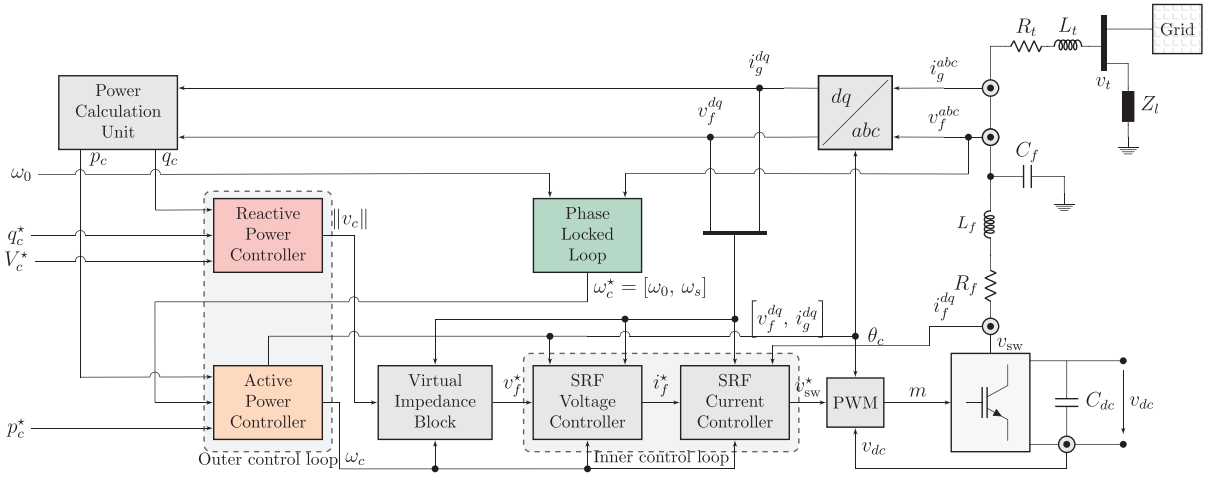

Fig. 1. General configuration of the implemented VSC control structure.

Table 1
Small-scale factors of the inverter model.

State variables	Small-scale factors Υ	
	Analytical expression	Numerical value
ξ^d, ξ^q	K_P^v/K_I^v	0.0008
v_f^d, v_f^q	$\omega_b \frac{\ell_f(\ell_g+\ell_t)}{r_d\left(\ell_f+\ell_g+\ell_t\right)}$	0.0152
$\tilde{p}_c$, $\tilde{q}_c$	$1/\omega_z$	0.0318
i_g^d, i_g^q	$\omega_b(\ell_g+\ell_t)/(r_g+r_t)$	0.0637
i_f^d, i_f^q	$\omega_b \ell_f / r_f$	0.0849
γ^d, γ^q	K_P^i/K_I^i	0.089
ε, θ_s, θ_c	1	1

previously described in D'Arco et al. [3], Markovic et al. [4], Ofir et al. [5], where the outer control loop consists of active and reactive power controllers providing the output voltage magnitude $\|v_c\| \in \mathbb{R}_{\geq 0}$ and frequency $\omega_c \in \mathbb{R}_{\geq 0}$ references by adjusting the predefined setpoints (denoted by *) according to a power imbalance. Assuming $p_c := v_f^\mathsf{T} i_g$ and $q_c := v_f^\mathsf{T} j^\mathsf{T} i_g$, follows:

$$\omega_c = \omega_c^\star + R_c^p(p_c^\star - \tilde{p}_c),\ v_c^d = V_c^\star + R_c^q(q_c^\star - \tilde{q}_c), \tag{21}$$

with $R_c^p \in \mathbb{R}_{\geq 0}$ and $R_c^q \in \mathbb{R}_{\geq 0}$ denoting the active and reactive power droop gains, $\tilde{p}_c \in \mathbb{R}$ and $\tilde{q}_c \in \mathbb{R}$ representing the low-pass filtered active and reactive power measurements given by

$$\dot{\tilde{p}}_c = \omega_z(p_c - \tilde{p}_c),\ \ \dot{\tilde{q}}_c = \omega_z(q_c - \tilde{q}_c), \tag{22}$$

and $\omega_z \in \mathbb{R}_{>0}$ being the cut-off frequency. Note that $v_c^q = 0$. The obtained reference voltage vector is passed through a virtual impedance block $(r_v, \ell_v) \in \mathbb{R}_{\geq 0}^2$, thus providing a minor cross-coupling between the d- and q-components via a grid current measurement $i_g \in \mathbb{R}_{\geq 0}^2$ at the converter terminal:

$$v_f^\star = v_c - (r_v + j\omega_c \ell_v) i_g. \tag{23}$$

The output is then fed to the inner control loop consisting of cascaded SRF voltage and current PI controllers:

$$i_f^\star = K_P^v(v_f^\star - v_f) + K_I^v \xi + K_F^v i_g + j\omega_c c_f v_f, \tag{24a}$$

$$v_{\text{sw}}^\star = K_P^i(i_f^\star - i_f) + K_I^i \gamma + K_F^i v_f + j\omega_c \ell_f i_f, \tag{24b}$$

with $\dot{\xi} = v_f^\star - v_f$ and $\dot{\gamma} = i_f^\star - i_f$ denoting the respective integrator states; $i_f^\star \in \mathbb{R}^2$ and $v_{\text{sw}}^\star \in \mathbb{R}^2$ represent the internally computed current and voltage references, $v_f \in \mathbb{R}^2$ and $i_f \in \mathbb{R}^2$ are the filter voltage and current, $(K_P^v, K_P^i) \in \mathbb{R}_{>0}^2$, $(K_I^v, K_I^i) \in \mathbb{R}_{\geq 0}^2$ and $(K_F^v, K_F^i) \in \mathbb{Z}_{\{0,1\}}^2$ are the proportional, integral and feed-forward gains respectively, and superscripts v and i denote the voltage and current SRF controllers. A type-2 PLL is used to detect the grid frequency $\omega_s \in \mathbb{R}_{\geq 0}$ at the connection terminal and keep the VSC synchronized via $\omega_c^\star = \omega_s$, thus operating in a so-called *grid-supporting* or *grid-following* mode [20]:

$$\omega_s = \omega_0 + K_P^s \hat{v}_f^q + K_I^s \varepsilon, \quad \dot{\varepsilon} = \hat{v}_f^q, \tag{25}$$

where ε denotes the integrator state, $\hat{v}_f = v_f e^{\theta_c - \theta_s}$, $\dot{\theta}_c = \omega_c \omega_b$ and $\dot{\theta}_g = \omega_g \omega_b$. The measured filter voltage v_f is transformed into an internal SRF of the PLL ($\hat{v}_f \in \mathbb{R}^2$) and passed through a PI controller $(K_P^s, K_I^s) \in \mathbb{R}_{>0}^2$ acting on the phase angle difference, therefore aligning the d-axis of the internal SRF with the stationary (abc)-frame; ω_0 denotes the nominal system frequency of 50 Hz, i.e., 1 p.u.

The electrical interface to the grid includes an *RLC* filter $(r_f, \ell_f, c_f) \in \mathbb{R}_{>0}^3$ and a transformer equivalent $(r_t, \ell_t) \in \mathbb{R}_{>0}^2$, modeled in SRF defined by the angular frequency ω_c:

$$\dot{i}_f = \omega_b \ell_f^{-1}(v_{\text{sw}} - v_f) - (\omega_b r_f \ell_f^{-1} + j\omega_b \omega_r) i_f, \tag{26a}$$

$$\dot{v}_f = \omega_b c_f^{-1}(i_f - i_g) - j\omega_b \omega_r v_f, \tag{26b}$$

$$\dot{i}_g = \omega_b \ell_t^{-1}(v_f - v_t) - (\omega_b r_t \ell_t^{-1} + j\omega_b \omega_r) i_g, \tag{26c}$$

with $v_{\text{sw}} \in \mathbb{R}^2$ and $v_t \in \mathbb{R}^2$ being the switching and terminal voltage. The system base frequency is represented by ω_b and equals the nominal frequency. The complete state-space model of a single grid-following inverter comprises 15 states of the form $\tilde{x}_c = (v_f^{dq}, i_f^{dq}, i_g^{dq}, \xi^{dq}, \gamma^{dq}, \varepsilon, \theta_c, \theta_s, \tilde{p}_c, \tilde{q}_c)$, whereas the grid-forming inverter model disregards the two PLL states (θ_s, ε). More details on the overall converter control structure and employed parametrization can be found in Markovic et al. [4], Ofir et al. [5], Markovic et al. [6], 21].

3.2. Timescale separation

A traditional approach in singular perturbation is to employ small parameters as an indicator of timescale separation within a dynamical system, since these factors are reflective of the time constants of individual state variables. In order to obtain such parameters, the differential equations describing the system dynamics must be reformulated such that the observed quantity is isolated on the left-hand side of the equation in the first-order form $\epsilon_i \dot{x}_i = x_i + \ldots$, with $\epsilon_i \in \Upsilon$ representing the respective time constant of the dynamics pertaining to the state variable x_i. The values of small parameters for the grid-connected inverter operating in a grid-following mode are given in Table 1, ordered respectively from the fastest to the slowest state variable. For mathematical validity, a small resistance $r_d = 0.02$ p. u. is added in series with the filter capacitor c_f. It should be noted that the grid-forming VSC experiences the same small parameters, with PLL states (θ_s, ε) being omitted from the model.

In contrast, through PFA approach the modes of the system are sorted by their natural frequency (i.e., the distance from the origin in the complex plane), defined as $\omega_k = \sqrt{\Re(\lambda_k)^2 + \Im(\lambda_k)^2}$. Subsequently, the states with the highest participation in the fastest mode (or conjugate pair of modes) are reduced, as indicated in Table 2. Such method suggests that the electrical states of the *RLC* filter within the device model, i.e., (v_f^d, v_f^q), (i_g^d, i_g^q) and (i_f^d, i_f^q) respectively, contribute the most to the fast modes and should be removed first in the given order. This is significantly different from the results in Table 1, where the integrator states of the SRF voltage control are prioritized over (v_f^d, v_f^q) and the dynamics of the outer control loop are faster than (i_g^d, i_g^q) and (i_f^d, i_f^q). The observed discrepancies between the two approaches indicate that the fastest states are not necessarily in direct correlation with the fastest modes, and removing them would not fully eliminate the less relevant modes. Similarly, the impact of fast variables on slower system dynamics might not be negligible, which is directly addressed through application of the FOSP methodology in the proposed hybrid approach.

The modal decomposition given in Table 2 shows that there are three modes of the system whose natural frequency is two orders of magnitude greater than the frequency of the slowest modes. Therefore,

Table 2
Modal analysis of the inverter model.

Eigenvalues	ω_k [Hz]	PF	Variables	ROM[a]
$-759.4 \pm j3684$	598.58	0.5188	v_f^d, v_f^q	13
$-649.4 \pm j3603$	582.67	0.3258	i_g^d, i_g^q	11
$-3530 \pm j348.2$	564.52	0.5112	i_f^d, i_f^q	9
$-32.6 \pm j194$	31.31	0.5495	ξ^d, ξ^q	7
-61.7	9.82	0.8924	θ_s	6
-31.5	5.01	1	$\tilde{q}_c$	5
$-10.1 \pm j29.2$	4.92	0.7167	$\tilde{p}_c$, θ_c	4,3
-12.6	2.01	0.8573	ε	2
-11.3[b]	1.79	1	γ	0

[a] After the removal of the corresponding state variables.
[b] A conjugate pair of eigenvalues with an imaginary part equal to zero.

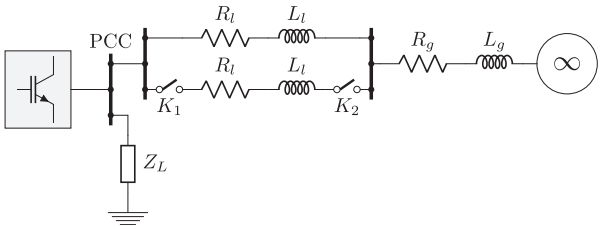

Fig. 2. Test case system comprising a single-line diagram of a converter connected to an infinite bus via two parallel transmission lines.

these modes can be considered very fast and the state variables with the highest participation should be removed using ZOSP. The dominant states contributing to the aforementioned modes are (v_f^d, v_f^q), (i_g^d, i_g^q) and (i_f^d, i_f^q). The remaining modes are separated at most by one order of magnitude and therefore are candidates for either ZOSP or FOSP. The time-domain performance for various combinations of ZOSP/FOSP reduction methods applied to the remaining state variables will be examined in Section 4.1.

4. Results

4.1. Time-domain performance during transients

In order to capture and compare the dynamic behavior and performance of different model orders and reduction methods during transients, we consider the test case illustrated in Fig. 2. It comprises a single inverter connected to a stiff grid (infinite bus) via two parallel transmission lines developed in MATLAB. In particular, the test case represents the disconnection of one of two parallel lines, effectively modeled through the opening of switches K_1 and K_2. The time-domain responses of different model orders for both grid-forming and grid-following operation mode are presented in Fig. 3, with full and dashed lines denoting the corresponding reductions using the zero-order and hybrid approach, respectively. The more oscillatory behavior of the grid-following unit is a consequence of the PLL. Additionally, in order to quantitatively benchmark the performance of each model, their run time and Root Mean Square Error (RMSE) in terms of active power and

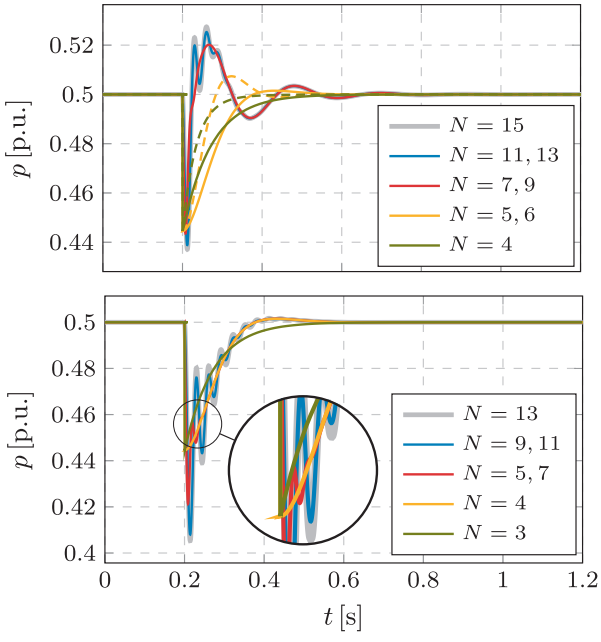

Fig. 3. Time-domain response of different model orders after line opening: (i) grid-following control mode; (ii) grid-forming control mode; dashed lines denote the corresponding reduction using the hybrid approach.

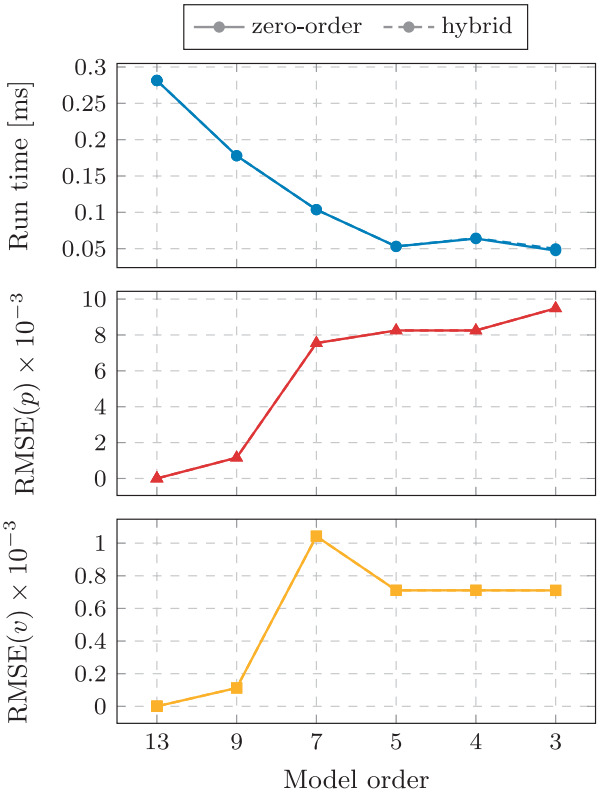

Fig. 4. Run time and RMSE for different model orders of grid-forming inverter using zero-order and hybrid approach.

voltage magnitude mismatch are computed and compared. For the purpose of generating a statistically relevant sample, the run time is computed as mean computational time over 100 iterations. On the other hand, the RMSE calculation is achieved by re-running the simulations for all model orders with a fixed-step solver and comparing the mismatch between signals at each discrete time step. Moreover, the RMSE metric is applied only to the period during transients, i.e., between the fault instance and the point at which the system reaches steady state, with the results depicted in Figs. 4 and 5.

It is immediately noticeable from Fig. 3 that dropping the very fast electrical states does not have much impact on the overall response. Indeed, after removing v_f and i_g the performance is unchanged for both operation modes, whereas only the very fast oscillations are not mapped by removing i_f. These findings therefore justify the use of zero-order reduction for the removal of very fast variables. Interestingly enough, dropping the integrator states (ξ^d, ξ^q) as next in line in Table 2 has no effect on the overall performance. While the corresponding mode is rather classified as fast than very fast, this effect might be explained by the fact that the time constant of the underlying state dynamics is very small (see Table 1). Moreover, as mathematical expressions for inner control loops are convoluted and nested, the elimination of state variables (ξ^d, ξ^q) was not possible using FOSP and resulted in numerical issues during model initialization. This is an important aspect and a potential drawback of a FOSP application to nonlinear systems, which has not been reported previously in Vorobev et al. [18]. Hence, the first 8 states are all removed using ZOSP, irrelevant of the inverter operation mode.

Going for lower-order models, we now tackle the relatively fast states, i.e., variables that could potentially be removed either using zero- or first-order reduction, with the use of the latter method resulting in the proposed hybrid MOR approach. For the grid-forming mode of operation there is a negligible difference in both the time-domain response and computational time when removing the remaining states with either ZOSP or FOSP. This can be seen both qualitatively in Fig. 3

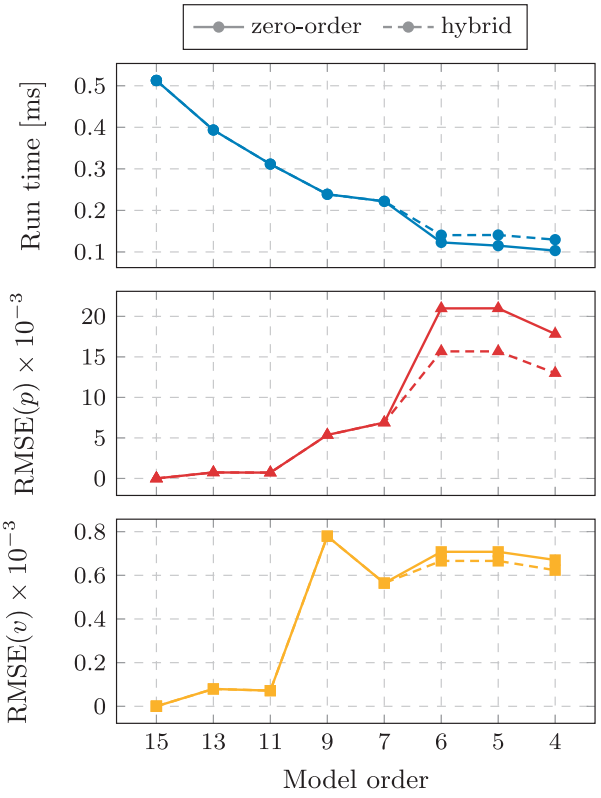

Fig. 5. Run time and RMSE for different model orders of grid-following inverter using zero-order and hybrid approach.

and quantitatively in Fig. 4. In both cases the fourth- and third-order models were derived with the hybrid model by removing $\tilde{q}_c$ and $\tilde{p}_c$, respectively. In general, applying either ZOSP or FOSP to the remaining two states does not pose a major factor, as all models experience a rather similar trajectory response, with the higher-order models showing initially larger deviation and oscillatory behavior. Thus, FOSP appears to offer no measurable improvement in this case; a somewhat understandable outcome considering that the zero-order approach already achieves a very accurate approximation of the full-order model, as previously observed in Cossart et al. [17].

While there is a negligible difference in the transient performance of a grid-forming inverter between the zero-order and hybrid approach, there is a significant improvement in the run time when reducing to fifth-order model and below. Despite an inevitable increase in RMSE, the significant reduction in run time makes these reduced order models appealing for large-scale system simulations. Indeed, similar model orders have also been proposed in Kodra et al. [9], Mariani et al. [10], Iyer et al. [11], Rasheduzzaman et al. [12], Luo and Dhople [13], Cossart et al. [17] using ZOSP.

For the case of grid-following operation, however, the reduced-order models below $N = 7$ presented in Fig. 3 show distinctly different behavior immediately following the disturbance. Any further reduction using ZOSP results in a lagged response and is incapable of reproducing the overshoot response of the full-order model. Although a seventh-order model may be sufficient for microgrid or small-scale analysis, it may be necessary to further reduce the model order for large-scale electro-magnetic transient simulations, particularly given the order of synchronous generator models and the relative capacity of converters and synchronous machines. For further reduction we consider two cases: the first, where we continue to reduce all states using ZOSP; and the second, where we adapt a hybrid approach by first removing θ_s using FOSP and all subsequent states using ZOSP. In both cases, the order of reduction is shown in Table 2. Namely, we see that the hybrid model, indicated by a dashed line, outperforms its corresponding ZOSP model as illustrated in Fig. 3. The hybrid model is better at reproducing the fast response of the full-order model, with both the hybrid sixth- and fifth-order models capturing the overshoot to a certain extent as well as the initial oscillatory behavior.

For the case of grid-following operation, there is a noticeable RMSE difference between the zero-order and the hybrid method, with ZOSP having $\approx 33\%$ higher RMSE in terms of active power response for the sixth-order and below (see Fig. 5). On the other hand, the run time is rather similar, especially for $N = 6$; a small difference is justified by the more complex nature of the first-order algebraic constraints in FOSP. Similarly to the grid-forming mode, a significant and steady reduction in the computational run time is observed when going for lower-order models, with sixth-order and lower being almost 50% faster than the model orders $N = 7$ and $N = 9$. This is again particularly advantageous when considering large system-scale simulations, where both computational time and memory allocation become a concern as the number of individual models scales up.

4.2. Eigenvalue analysis & stability properties

Some interesting observations can be made by studying the most critical modes of the root loci spectrum for different model orders of the zero-order approach, depicted in Fig. 6. Understandably, removing states associated with very fast dynamics has no impact on the slow modes, reflected in the preserved eigenvalue spectrum close to the imaginary axes for $N \geq 7$. Nevertheless, dropping the dynamics of the outer control loop (i.e., $\tilde{q}_c$ and $\tilde{p}_c$ respectively) and PLL (i.e., θ_s) has a massive impact on the slow modes. In particular, the most critical pair of eigenvalues is significantly shifted to the left, whereas other slow modes now become more critical. This "movement" is indicated by the dashed lines in Fig. 6. Such massive changes in the root loci spectrum might also justify the changes in the transient performance and drastic increase in RMSE when going for $N < 7$, especially in the case of a grid-following inverter due to the presence of a PLL.

These conclusions are substantiated by the stability maps provided in Fig. 7, defining a stable region in the $R_c^p - R_c^q$ plane. Different lines indicate a change in the boundary of the stable region for the corresponding model order. It should be noted that for lower orders ($N \leq 6$), the whole region of interest is stable and the lines are therefore not graphically illustrated. These results are in direct correlation with Fig. 6. More precisely, the mismatch between the slow modes of the full- and reduced-order models is mapped to the accuracy of the approximation of the stable region boundary, with a massive shift in the critical modes for $N = 6$ reflected by a very large stable region. Such change is not surprising, considering that the removed states affect the dynamics of active and reactive power control, and the stability region of interest is analyzed in the $R_c^p - R_c^q$ plane. It however highlights that both ZOSP and FOSP might not be applicable to stability studies when

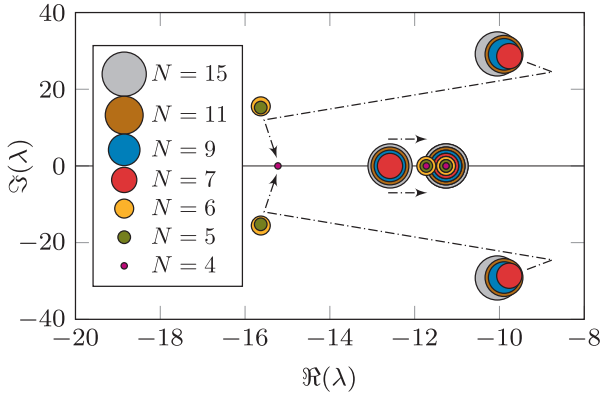

Fig. 6. Root loci spectrum of interest for different model orders using zero-order reduction of a grid-following inverter.

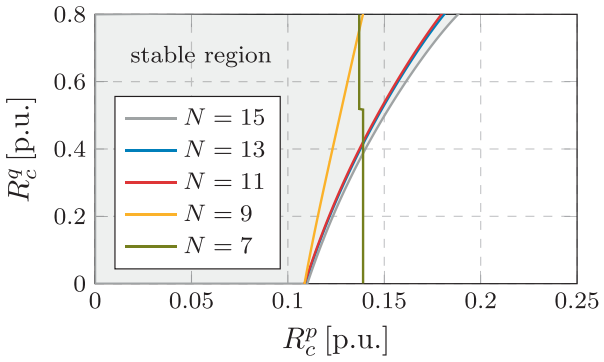

Fig. 7. Stability maps corresponding to different model orders of grid-following inverter in Fig. 6; the system is stable within the shaded region.

reaching lower-order inverter models (especially with the use of PFA), which was not reported in Vorobev et al. [18] as this study dealt with a very low full-order model.

Furthermore, the discrepancies in the approximation of the stability region suggest that different modeling approaches and model orders should be employed when dealing with small-signal analysis compared to the simulations of large-signal disturbances (e.g., line openings and short circuits). In particular, while PFA seems promising in terms of defining the most relevant states for preserving the transient response of the original model, it does not always respect the timescales of the system and could potentially violate the necessary stability conditions for singular perturbation theory. On the other hand, the traditionally used small parameters might fail to capture the fast transients of the full-order model. Therefore, alternative metrics such as controllability and observability of the modes and their respective residues could be employed in determining the optimal reduced model order.

5. Conclusion

This paper presents a hybrid model-order reduction method, which takes advantage of different timescales in a dynamical model and can be applied to nonlinear systems. In particular, it combines the low computational burden of the traditional zero-order singular perturbation with the higher accuracy of the first-order approach. In order to determine the order of the state removal, the conventional method based on small parameters is replaced by an iterative participation factor analysis. The novel hybrid approach is applied to both grid-forming and grid-following inverter control schemes, and compared against the traditional zero-order reduction. While the improvement in the performance of the lower-order models of the grid-forming inverter is insignificant, the results for the grid-following operation mode showcase a better time-domain performance during transients, while having only a negligible increase in computational requirements.

Future work will focus on the performance of the hybrid reduction method in a large-scale network with a high penetration of inverter-interfaced generation. The slower dynamics of conventional generation as well as the very fast dynamics of transmission lines are expected to have a significant influence on the acceptable model order. The mix of different system dynamics can be effectively tackled by the proposed reduction technique and presents an interesting path for future studies.

Declaration of Competing Interest

The authors declare that they have no known competing financial interests or personal relationships that could have appeared to influence the work reported in this paper.

References

[1] F. Milano, F. Dörfler, G. Hug, D.J. Hill, G. Verbič, Foundations and challenges of low-inertia systems, PSCC, (2018).
[2] N. Pogaku, M. Prodanovic, T.C. Green, Modeling, analysis and testing of autonomous operation of an inverter-based microgrid, IEEE Trans. Power Electron. 22 (2) (2007) 613–625.
[3] S. D'Arco, J.A. Suul, O.B. Fosso, Small-signal modelling and parametric sensitivity of a virtual synchronous machine, PSCC, (2014).
[4] U. Markovic, J. Vorwerk, P. Aristidou, G. Hug, Stability analysis of converter control modes in low-inertia power systems, IEEE Innovative Smart Grid Technologies - Europe (ISGT-Europe), (2018).
[5] R. Ofir, U. Markovic, P. Aristidou, G. Hug, Droop vs. virtual inertia: Comparison from the perspective of converter operation mode, IEEE International Energy Conference (ENERGYCON), (2018).
[6] U. Markovic, O. Stanojev, P. Aristidou, G. Hug, Partial grid forming concept for 100% inverter-based transmission systems, IEEE PES General Meeting, (2018).
[7] Y. Lin, B. Johnson, V. Gevorgian, V. Purba, S. Dhople, Stability assessment of a system comprising a single machine and inverter with scalable ratings, NAPS, (2017).
[8] H.K. Khalil, Nonlinear Systems, third ed., Prentice Hall, 2002.
[9] K. Kodra, N. Zhong, Z. Gajić, Model order reduction of an islanded microgrid using singular perturbations, ACC, (2016).
[10] V. Mariani, F. Vasca, J.M. Guerrero, Analysis of droop controlled parallel inverters in islanded microgrids, 2014 IEEE International Energy Conference (ENERGYCON), (2014).
[11] S.V. Iyer, M.N. Belur, M.C. Chandorkar, A generalized computational method to determine stability of a multi-inverter microgrid, IEEE Trans. Power Electron. 25 (9) (2010) 2420–2432.
[12] M. Rasheduzzaman, J.A. Mueller, J.W. Kimball, Reduced-order small-signal model of microgrid systems, IEEE Trans. Sustain. Energy 6 (4) (2015) 1292–1305.
[13] L. Luo, S.V. Dhople, Spatiotemporal model reduction of inverter-based islanded microgrids, IEEE Trans. Energy Convers. 29 (4) (2014) 823–832.
[14] S. Curi, D. Groß, F. Dörfler, Control of low-inertia power grids: a model reduction approach, IEEE Conference on Decision and Control (CDC), (2017), pp. 5708–5713.
[15] G. Peponides, P. Kokotovic, J. Chow, Singular perturbations and time scales in nonlinear models of power systems, IEEE Trans. Circuits Syst. 29 (11) (1982) 758–767.
[16] P. Kokotovic, H.K. Khali, J. O'reilly, Singular Perturbation Methods in Control: Analysis and Design, 25 Siam, 1999.
[17] Q. Cossart, F. Colas, X. Kestelyn, Model reduction of converters for the analysis of 100% power electronics transmission systems, International Conference on Industrial Technology (ICIT), (2018).
[18] P. Vorobev, P. Huang, M.A. Hosani, J.L. Kirtley, K. Turitsyn, High-fidelity model order reduction for microgrids stability assessment, Trans. Power Syst. 33 (2018) 874–887.
[19] I.J. Perez-Arriaga, G.C. Verghese, F.C. Schweppe, Selective modal analysis with applications to electric power systems, part I: heuristic introduction, IEEE Power Eng. Rev. PER-2 (9) (1982) 29–30, https://doi.org/10.1109/MPER.1982.5519461.
[20] J. Rocabert, A. Luna, F. Blaabjerg, P. Rodríguez, Control of power converters in ac microgrids, IEEE Trans. Power Electron. 27 (11) (2012) 4734–4749.
[21] Markovic U., Stanojev O., Vrettos E., Aristidou P., Callaway D., Hug G., Understanding stability of low-inertia systems, IEEE Trans. Power Syst. (under review)., doi:10.31224/osf.io/jwzrq.